Atmospheric Environment 274 (2022) 118958

Contents lists available at ScienceDirect

Atmospheric Environment

journal homepage: www.elsevier.com/locate/atmosenv

Characteristics and formation mechanisms of atmospheric carbonyls in an oilfield region of northern China

Tianshu Chen [a], Penggang Zheng [a], Yingnan Zhang [a], Can Dong [a], Guangxuan Han [b], Hong Li [c], Xue Yang [d], Yuhong Liu [a], Jingjing Sun [a], Hongyong Li [a], Xin Zhang [a,c], Yunfeng Li [e], Wenxing Wang [a,c], Likun Xue [a,*]

[a] Environment Research Institute, Shandong University, Qingdao, 266237, China
[b] Key Laboratory of Coastal Environmental Process and Ecology Remediation, Yantai Institute of Coastal Zone Research, Chinese Academy of Sciences, Yantai, 264003, China
[c] Chinese Research Academy of Environmental Sciences, Beijing, 100012, China
[d] School of Municipal and Environmental Engineering, Shandong Jianzhu University, Jinan, 250101, China
[e] School of Mechanical Engineering, Beijing Institute of Petrochemical Technology, Beijing, 102617, China

HIGHLIGHTS

- This study presents for the first-time detailed characteristics of carbonyls in a typical oilfield region of China.
- The strong in-situ production of formaldehyde and acetaldehyde in the YelRD region was demonstrated.
- The strong oilfield emissions affect the formation mechanisms of carbonyls.

ARTICLE INFO

Keywords:
Carbonyl compounds
Oilfield
Chemical budget
Master Chemical Mechanism
Yellow River Delta region

ABSTRACT

Oil and natural gas (O&NG) associated oxygenated volatile organic compounds (OVOCs) have been reported to play a significant role in ozone formation. However, little is known about the characteristics of O&NG-related OVOCs and their environmental impacts in China. In this work, C_1–C_8 carbonyls, an important member of the OVOCs family, were measured at a rural site and an oilfield in the Yellow River Delta region (YelRD) in winter and summer 2017. The well-defined seasonal (higher in summer) and diurnal variation (peak in the afternoon) patterns of carbonyls indicated a significant influence of secondary formation. Spatially, the measured carbonyls showed higher concentrations in the oilfield than in the rural air due to the strong oilfield emissions of hydrocarbon precursors. The chemical budget and formation mechanisms of formaldehyde and acetaldehyde were explored with the application of an observation-based model coupled with Master Chemical Mechanism. Alkenes (including both anthropogenic and biogenic species) played dominant roles in the secondary formation of formaldehyde both in the oilfield and in the rural area. Seasonally, anthropogenic alkenes showed the highest positive relative incremental reactivity (RIR) for formaldehyde within most winter-cases, while biogenic alkenes showed the highest positive RIR in summer. Spatially, anthropogenic hydrocarbon precursors showed larger RIR values in the oilfield than in the rural area. This study presents for the first-time detailed characteristics of carbonyls in a typical oilfield region of China and quantitatively reveals the impacts of oilfield emissions on the photochemical formation of major carbonyl compounds.

1. Introduction

Energy is an important pillar of human development. From the perspective of energy structure, oil and natural gas (O&NG) have been playing a dominant role since the 19th century. The main uses of O&NG include the production of secondary energy sources (such as gasoline, diesel, and liquefied petroleum gas) and chemical products. Despite the development of new energy, the O&NG production has been increasing

* Corresponding author.
E-mail address: xuelikun@sdu.edu.cn (L. Xue).

https://doi.org/10.1016/j.atmosenv.2022.118958
Received 14 November 2021; Received in revised form 10 January 2022; Accepted 14 January 2022
Available online 20 January 2022
1352-2310/© 2022 Elsevier Ltd. All rights reserved.

globally with the increased importance of petrochemicals in driving oil demand growth. According to the BP Statistical Review of World Energy (British Petroleum Company plc, 2020), O&NG accounted for 57.3% of global primary energy consumption in 2019. O&NG production emits abundant air pollutants, especially volatile organic compounds (VOCs), into the ambient environment, hindering the improvement of air quality and public health at different scales (Adgate et al., 2014; Colborn et al., 2013; Field et al., 2015; McDuffie et al., 2016).

Oxygenated volatile organic compounds (OVOCs) are reactive VOCs with oxygen-containing functional groups, and carbonyls (with a C═O moiety) are important members of the OVOCs family (Mellouki et al., 2015). The dominant loss mechanisms of OVOCs are reactions with OH radicals and photolysis, both of which play an essential role in peroxy radical (HO_2 and RO_2) production and atmospheric oxidation chemistry (Xue et al., 2016). Such pathway makes OVOCs an important contributor to the photochemical formation of tropospheric ozone (O_3), an important air pollutant and a greenhouse gas (Zhang et al., 2019; Mellouki et al., 2015). As such, many observational and observation-based modeling studies have been conducted to investigate the characteristics and formation mechanisms of OVOCs in various environments around the world, covering urban, semi-urban, rural and remote areas (Cheng et al., 2014; Jiang et al., 2016; Mu et al., 2007; Wang et al., 2020; Wu et al., 2020; Yang et al., 2018; Ye et al., 2021; Zhang et al., 2019).

During the entire lifetime of O&NG energy (e.g., production, processing, storage, transport, and use of fuels and chemical products), carbonyls can be emitted directly or formed by the photochemical oxidation of parent hydrocarbons (Mellouki et al., 2015; McDonald et al., 2018; Zhang et al., 2019). Several studies have reported abnormally high wintertime O_3 concentrations in U.S. O&NG producing regions, which were attributed to the combined effects of adverse weather conditions and chemical processes (Edwards et al., 2014; Ahmadov et al., 2015). From a chemistry point of view, the role of carbonyl compounds is highlighted. For example, Edwards et al. (2014) attributed 85% of modeled radical sources to carbonyl photolysis in wintertime O_3 pollution events in the O&NG producing area of northeastern Utah, the U.S. Barickman and Lyman (2015) reported that carbonyls were emitted from equipment used by the O&NG production in the Uintah Basin, the U.S. However, to our best knowledge, no studies have systematically investigated the composition, characteristics, and formation mechanisms of carbonyls emitted or generated in the oilfield regions of China, which has been suffering from haze and photochemical air pollution in recent decades.

China ranked the 7th in oil production and the 6th in natural gas production worldwide in 2018 (EIA, 2021a; EIA, 2021b). It is expected that the O&NG-associated activities exert significant impacts on regional air quality. However, few studies have evaluated the impacts of O&NG-related activities on regional air quality in China. Our previous study reported severe O_3 episodes in an open oilfield region of northern China, and chemical box modelling analyses revealed that the abundant OVOCs drove the radical recycling efficiently under low-NO_x conditions and hence promoted O_3 formation (Chen et al., 2020). This work is a follow-up study of Chen et al. (2020), focusing on the detailed tempo-spatial variations and formation mechanisms of major carbonyls in the same oilfield region. Here we first present the carbonyl measurements at a rural site near the O&NG production region in winter and summer 2017. The seasonal variations, diurnal variations, and spatial distributions of C_1–C_8 carbonyl species are analyzed. The formation mechanisms of the most abundant carbonyl species (i.e., formaldehyde and acetaldehyde) are then explored, and the impacts of oilfield emissions on the secondary formation of carbonyls are finally discussed. The findings provide insights into the characteristics, sources, and air quality impacts of carbonyls in typical oilfield regions of China.

2. Methods

2.1. Field experiments

The Yellow River Delta (YelRD) region covers the Dongying city (approximately 300 km southeast of Beijing) and its surrounding areas, and hosts the fifth largest oilfield of China (Fig. 1). Field observations were carried out in winter (from February 9 to March 31) and summer (from 1 June to 10 July) 2017 at the YelRD Ecological Research Station of Coastal Wetland (37.76°N, 118.98°E, 0 m above sea level), Chinese Academy of Sciences. This rural site is surrounded by open oilfields and there are no evident anthropogenic emissions nearby. The southerly and southeasterly winds prevail in summer, while northerly winds prevail in winter. The site is generally located at the downwind of downtown Dongying (roughly 32 km away) and the major oilfield area in summer, and at the downwind of another large concentrated oilfield area in winter (see Fig. 1). During the summer campaign, an oilfield site was set up in the oilfield area, upwind (southwest) of the rural site, for collection of carbonyl and VOC samples exactly in the oilfield source areas. Especially, simultaneous intensive sampling was carried out at both sites during an episode of July 9, 2017. Detailed information about the field campaigns can be found in Chen et al. (2020).

Ambient air samples were collected at the rural site in the daytime (from 07:00 to 19:00 LT, with an interval of approximately 2 h) during selected $PM_{2.5}$ pollution episodes in winter (i.e., February 19, 22, 23, 27, 28 and March 11, 23, 29) as well as in the daytime (from 06:00 to 18:00 LT, with an interval of 2 h) during selected O_3 pollution episodes (i.e., June 8, 9, 14, 15, 16, 18, 29, 30 and July 9) in summer. The $PM_{2.5}$ or O_3 pollution episodes were predicted according to the air quality model forecast. In addition, air samples were also collected 1–3 times each day during the remaining period without wet precipitation. A total of 129 samples were collected at the rural site. Additional air samples were collected on June 26 (4 samples) and July 9 (6 samples) at the oilfield site. The time series of carbonyls and related species during the sampling days were provided in the SI. For carbonyls, the air sample was absorbed in a 2,4-dinitrophenylhydrazine-coated sorbent cartridge (*Waters Sep-Pak DNPH–silica*) and analyzed with the high-performance liquid chromatography (HPLC) to quantify 15 C_1–C_8 carbonyl species (e.g., formaldehyde, acetone, acetaldehyde, n-valeraldehyde, n-butyraldehyde, crotonaldehyde, hexaldehyde, propionaldehyde, 2,5-dimethyl benzaldehyde, p-tolualdehyde, benzaldehyde, i-valeraldehyde, m-tolualdehyde, acraldehyde, o-tolualdehyde). VOC canister samples were collected simultaneously with carbonyl samples. Details about the VOC sampling and detection as well as real-time measurements and time series of other parameters (including trace gases, aerosols, and meteorological parameters) were described in Chen et al. (2020).

2.2. Chemical box model

An observation-based model (OBM) was used to diagnose the formation mechanisms (mainly chemical budget and relationships with precursors) of formaldehyde and acetaldehyde. The OBM was run based on the Framework for zero-dimensional Atmospheric Modeling (F0AM) platform (Wolfe et al., 2016). The adopted chemical mechanism was Master Chemical Mechanism (MCM) version 3.3.1, which near-explicitly describes the chemical degradation pathways of 143 primary VOC species (Saunders et al., 2003). Detailed information about model setup can be found in Chen et al. (2020).

During the simulation, the OBM was constrained by the observed data of NO, NO_2, HONO, O_3, SO_2, CO, CH_4, C_2–C_{10} NMHCs, and C_1–C_8 carbonyls concentrations, temperature, relative humidity (RH), and the photolysis frequency of NO_2 (J_{NO2}), which were processed into 1-hr time resolution. For both rural and oilfield sites, the 1-hr resolution daytime CH_4, C_2–C_{10} NMHCs, and carbonyl concentrations were obtained by interpolation. For the nighttime data, the concentrations of CH_4 and C_2–C_{10} NMHCs (except for isoprene, α-pinene, and β-pinene) were

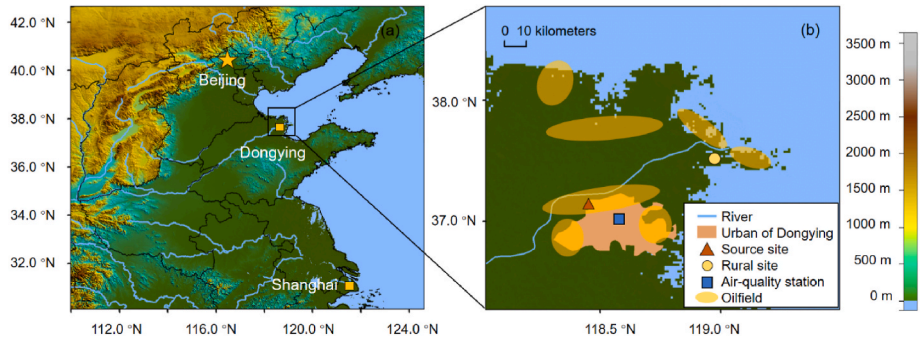

Fig. 1. Maps showing the locations of (a) Yellow River Delta region; (b) the rural site, the oilfield site, and the oilfield areas. (For interpretation of the references to colour in this figure legend, the reader is referred to the Web version of this article.)

extrapolated into 1-hr time resolution according to the linear relationship with CO; the concentrations of isoprene, α-pinene and β-pinene were extrapolated according to the linear relationship with temperature; and the carbonyl concentrations were extrapolated based on the multiple linear regressions with CO and O_3. The purpose of extrapolating nighttime data was to facilitate the constant run of the model, and would not exert significant effects on simulation results during the daytime. Observed data of trace gases (e.g., NO_2, O_3, SO_2, and CO concentrations) and meteorological parameters (e.g., temperature, RH, and J_{NO2}) were unavailable for the oilfield site and were processed as follows. The observed data of trace gases were obtained from the closest national air-quality monitoring station (the location was marked in Fig. 1), and the meteorological parameters were assumed to be the same to the rural site. For simulation of each episode (eleven cases for the rural site and one case for the oilfield site), the model was pre-run for 3 days to stabilize the concentrations of unmeasured species and the results from the 4th day were extracted for analyses.

The method for quantifying the chemical budget of formaldehyde and acetaldehyde was elucidated in detail in Yang et al. (2018). A brief introduction is given here. The reactions related to the formation of formaldehyde and acetaldehyde were explicitly tracked in the model and grouped into several major pathways according to E1 and E2. The production rate of formaldehyde was calculated as the sum of reaction rates for $O_2 + CH_3O$, O_2 + RO (resulting from alkenes), O_2 + RO (resulting from other VOCs), O_3 + VOCs and other reactions (e.g., cross-radical reactions and photolysis of OVOCs, OH + OVOCs):

$$\mathrm{P}(formaldehyde) = k_1[O_2][CH_3O] + \sum(k_{2i}[O_2][RO_i(from\ alkenes)]) + \sum(k_{3i}[O_2][RO_i(from\ other\ VOCs]) + \sum(k_{4i}[O_3][VOC_i]) + \sum(other\ reactions) \quad \text{(E1)}$$

The production rate of acetaldehyde was calculated as the sum of reaction rates for $O_2 + C_2H_5O$, O_2 + RO (from alkenes), O_2 + RO (from other VOCs), O_3 + VOCs, OH + OVOCs, and other reactions (e.g., cross-radical reactions and photolysis of OVOCs):

$$\mathrm{P}(acetaldehyde) = k_5[O_2][C_2H_5O] + \sum(k_{6i}[O_2][RO_i(from\ alkenes)]) + \sum(k_{7i}[O_2][RO_i(from\ other\ VOCs]) + \sum(k_{8i}[O_3][VOC_i]) + \sum(k_{9i}[OH][OVOC_i]) + \sum(other\ reactions) \quad \text{(E2)}$$

The chemical loss rates of formaldehyde and acetaldehyde were calculated as the sum of reaction rates for photolysis of carbonyl species, carbonyl + OH, and carbonyl + NO_3 (E3). Here carbonyl was used to refer to the target carbonyl species (i.e., formaldehyde or acetaldehyde).

$$\mathrm{L}(carbonyl) = j_1[carbonyl] + k_{10}[carbonyl][OH] + k_{11}[carbonyl][NO_3] \quad \text{(E3)}$$

The net production rate can be quantified as the difference between the total production rate and the total loss rate:

$$\text{net}\ \ \mathrm{P}(carbonyl) = \mathrm{P}(carbonyl) - \mathrm{L}(carbonyl) \quad \text{(E4)}$$

Details about the lumping of chemical formation and loss pathways have been described in Yang et al. (2018). Previous studies have demonstrated the important role of halogens on the fate of VOCs and OVOCs, radical budget, and atmospheric oxidative capacity in the coastal region (Xue et al., 2015). However, due to the limitation of available observation data for halogens, the influence of Cl reactions on carbonyl formation mechanism was not considered in this study, which warrants more investigations in the future.

A series of sensitivity model runs were conducted to quantify the relationship between formaldehyde formation and its major precursor groups. The acetaldehyde was excluded due to its low net production rates as shown in Section 3.2. The formaldehyde-precursor relationship was evaluated by a metric of relative incremental reactivity (RIR), which is defined as the ratio of the change in net production rate of formaldehyde to changes in its precursor concentrations (i.e., a 20% reduction in this study). The precursors were grouped into 8 categories, namely, NO_x, C_2–C_5 alkanes, C_6–C_{10} alkanes, C_2–C_5 anthropogenic alkenes (hereafter referred to as A-alkenes), biogenic alkenes (B-alkenes; including isoprene, α-pinene, and β-pinene), alkyne, BTEX (including benzene, toluene, ethylbenzene, and xylenes), and other aromatics. In

Table 1
Descriptive statistics of measured C_1–C_8 carbonyls at rural and oilfield site in the Yellow River Delta region in 2017.

Compound	Rural site Winter		Rural site Summer		Oilfield site June 26 & July 7	
	Mean ± SD (ppbv)	Mean Contrib. (%)	Mean ± SD (ppbv)	Mean Contrib. (%)	Mean ± SD (ppbv)	Mean Contrib. (%)
Formaldehyde	3.17 ± 2.12	23.4	8.59 ± 3.37	30.2	11.37 ± 3.69	34.9
Acetone	4.05 ± 3.1	30.4	6.86 ± 2.23	25.3	7.69 ± 3.88	21.7
Acetaldehyde	2.38 ± 1.5	17.8	5.31 ± 2.42	18.5	9.05 ± 6.71	22.8
n-Valeraldehyde	0.09 ± 0.06	0.9	1.89 ± 1.28	6.6	1.35 ± 2.05	2.4
n-Butyraldehyde	0.43 ± 0.2	3.5	1.85 ± 0.64	6.7	2.36 ± 2.06	5.6
Crotonaldehyde	1.78 ± 1.51	16.1	0.84 ± 1.01	2.9	0.62 ± 0.21	2.1
Hexaldehyde	0.18 ± 0.11	1.7	0.81 ± 0.97	2.6	0.83 ± 0.71	2.6
Propionaldehyde	0.24 ± 0.15	2.0	0.56 ± 0.26	2.0	1.12 ± 0.66	3.1
2,5-Dimethyl benzaldehyde	0.03 ± 0.07	0.4	0.46 ± 1.35	1.1	0.05 ± 0.01	0.2
p-Tolualdehyde	0.04 ± 0.05	0.5	0.43 ± 0.49	1.5	0.80 ± 0.34	2.7
Benzaldehyde	0.17 ± 0.14	1.5	0.25 ± 0.11	0.9	0.27 ± 0.11	0.8
i-Valeraldehyde	0.05 ± 0.05	0.6	0.10 ± 0.14	0.8	0.10 ± 0.04	0.3
m-Tolualdehyde	0.04 ± 0.05	0.5	0.09 ± 0.10	0.3	0.08 ± 0.01	0.3
Acraldehyde	0.06 ± 0.05	0.6	0.07 ± 0.03	0.3	0.12 ± 0.07	0.4
o-Tolualdehyde	0.02 ± 0.01	0.3	0.05 ± 0.01	0.2	0.08 ± 0.01	0.3
Total	12.75 ± 5.63	100.0	28.18 ± 10.74	100.0	35.90 ± 18.63	100.0

Mean Contrib.: Mean contribution of the compound to the total concentration of measured carbonyls.

this study, the B-alkenes was classified into biogenic source VOCs, while the other VOCs groups were classified into anthropogenic source VOCs.

3. Results and discussion

3.1. General characteristics of C_1–C_8 carbonyls

Table 1 lists the descriptive statistics of C_1–C_8 carbonyls observed both in winter, summer of rural site and summer of oilfield site. The average concentrations (±standard deviation) of summed C_1–C_8 carbonyls were 12.75 ± 5.63, 28.18 ± 10.74, and 35.90 ± 18.63 ppbv at the rural site in winter and summer and at the oilfield site in summer, respectively. Formaldehyde, acetone, and acetaldehyde were the most abundant carbonyl species, all of which accounted for 71.6 ± 15.5%, 74.0 ± 7.0%, and 79.4 ± 3.7% to the total observed C_1–C_8 carbonyls at the rural site in winter and summer and at the oilfield site in summer, respectively. In comparison, the other 12 species only composed a relatively small fraction (28.4 ± 15.5%, 26.0 ± 7.0%, and 20.6 ± 3.7% at the rural site in winter and summer and at the oilfield site in summer) of total C_1–C_8 carbonyls. Such chemical compositions were generally consistent with those measured in most urban, sub-urban, and rural areas from previous studies (Bao et al., 2022; He et al., 2020; Liu et al., 2021; Wang et al., 2020; Zhang et al., 2019).

The measurement data (in summer) at the rural site and at the oilfield site were compared to elucidate the influence of O&NG production on the carbonyl pollution. The total concentrations of C_1–C_8 carbonyls were higher in the oilfield source region than in the rural air (35.90 ± 18.63 ppbv vs. 28.18 ± 10.74 ppbv). Such spatial distribution was as expected considering the strong emissions and higher abundances of major C_1–C_{10} hydrocarbons in the oilfields (184.1 ± 186.5 ppbv vs. 29.7 ± 30.3 ppbv in the rural air; Chen et al., 2020). To eliminate the influence of meteorological conditions, we also compared the concurrent observation case on July 9, and the same spatial distribution pattern was obtained. For major carbonyls, the concentrations of formaldehyde, acetaldehyde, and acetone were all higher at the oilfield site (11.37 ± 3.69 ppbv, 9.05 ± 6.71 ppbv, and 7.69 ± 3.88 ppbv, respectively) than at the rural site (8.59 ± 3.37 ppbv, 5.31 ± 2.42 ppbv, and 6.86 ± 2.23 ppbv), though the enhancement degree varied. As a result, the contributions of formaldehyde and acetaldehyde to total C_1–C_8 carbonyls were relatively higher, while those of acetone were lower at the oilfield site (34.9 ± 9.3%, 22.8 ± 5.3%, and 21.7 ± 2.7%) than at the rural site (30.2 ± 4.4%, 18.5 ± 2.9% and 25.3 ± 5.0%). The measurement data of these three major carbonyl species in the rural area of YelRD were also compared with those from other studies (Table 2), and their concentration levels were comparable to those observed in polluted areas of China such as Beijing (Huang et al., 2020; Qian et al., 2019), Shanghai (Liu et al., 2019), Shenzhen (Huang et al., 2020), and Chengdu (Bao et al., 2022), and were substantially higher than those observed in sub-rural and rural areas of France (Jiang et al., 2016; Michoud et al., 2017) and urban areas of Spain (Villanueva et al., 2021) and Brazil (Nogueira et al., 2017). The above results reveal the severe carbonyl pollution in the YelRD region and demonstrate the significant impact of oilfield emissions.

The observation data at the rural site between in summer and in winter were compared to elucidate the seasonal variation of carbonyls in the YelRD region. The total concentrations of C_1–C_8 carbonyls were

Table 2
Overview of the measured formaldehyde, acetaldehyde, and acetone in this work and comparisons with other studies.

Location	Site type	Period	Formaldehyde (ppbv)	Acetaldehyde (ppbv)	Acetone (ppbv)	Reference
Dongying, China	Rural	2017.6–7	8.59 ± 3.37	5.31 ± 2.42	6.86 ± 2.23	This study
Dongying, China	Rural	2017.2–3	3.17 ± 2.12	2.38 ± 1.50	4.05 ± 3.10	This study
Shanghai, China	Urban	2017.5	3.17 ± 1.29	1.28 ± 0.68	–	Liu et al., (2019)
Shenzhen, China	Sub-urban	2018.4	1.60 ± 0.86	1.16 ± 0.90	2.31 ± 1.32	Huang et al., (2020)
Beijing, China	Urban	2018.5–6	6.31 ± 2.79	2.90 ± 1.36	4.16 ± 1.44	Huang et al., (2020)
Beijing, China	Urban	2015.8	6.90 ± 2.93	2.57 ± 1.20	4.61 ± 1.73	Qian et al., (2019)
Beijing, China	Urban	2018.7–8	8.49 ± 2.11	2.97 ± 0.79	6.72 ± 1.58	Qian et al., (2019)
Chengdu, China	Urban	2019.8	9.86 ± 4.41	3.57 ± 2.19	4.41 ± 2.32	Bao et al., (2022)
São Paulo, Brazil	Urban	2016	3.70 ± 1.30	2.80 ± 1.50	–	Nogueira et al., (2017)
Ciudad Real, Spain	Urban	2015.4–5	2.05 ± 0.70	1.30 ± 0.70	1.19 ± 0.88	Villanueva et al., (2021)
Ciudad Real, Spain	Urban	2015.6–9	2.97 ± 0.67	1.62 ± 0.45	3.51 ± 1.85	Villanueva et al., (2021)
Orléans, France	Sub-urban	2011.4	2.16 ± 0.59	1.02 ± 0.28	2.08 ± 0.72	Jiang et al., (2016)
Orléans, France	Sub-urban	2011.6–7	3.08 ± 2.21	1.04 ± 0.50	2.00 ± 1.12	Jiang et al., (2016)
Bastia, France	Rural	2013.6–8	2.48 ± 0.87	0.33 ± 0.12	3.43 ± 1.13	Michoud et al., (2017)

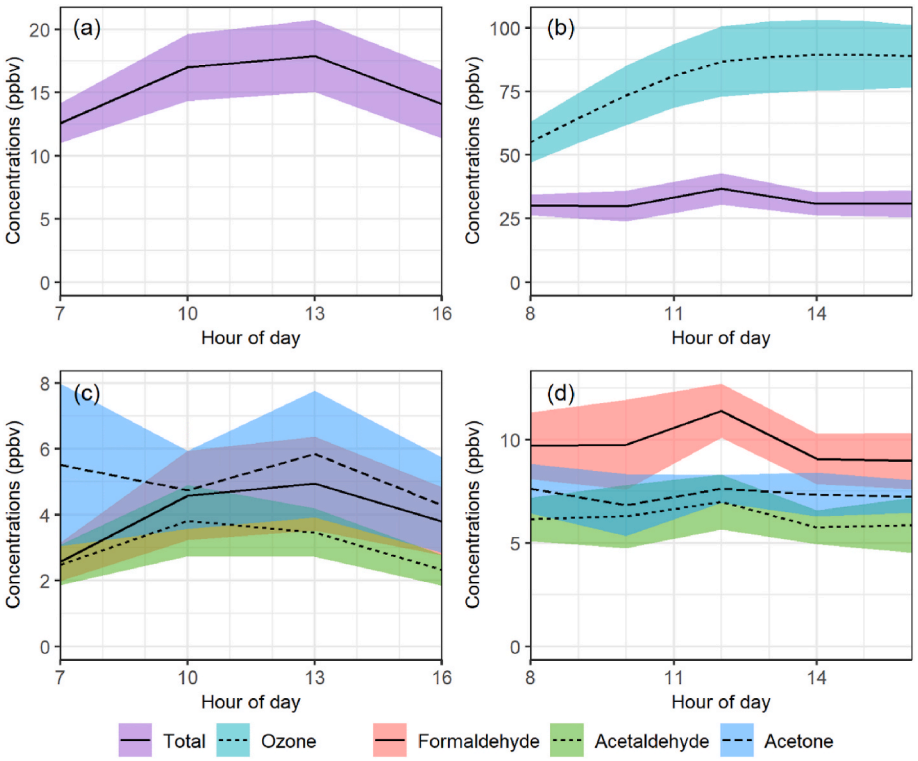

Fig. 2. Average daytime variations of C_1–C_8 carbonyls in (a) winter and (b) summer, and major compounds (formaldehyde, acetaldehyde, and acetone) in (c) winter and (d) summer at the rural site. The shadows indicate the **half** standard deviation of the mean concentrations. Sampling days with only one samples one were excluded. Time points with only one sample during the campaign were also excluded (Data source of O_3: Chen et al. (2020)).

significantly higher in summer than in winter (28.18 ± 1.74 ppbv versus 12.75 ± 5.63 ppbv; $p < 0.01$). Such seasonal pattern was opposite to that of C_1–C_{10} hydrocarbons but was consistent to that of O_3, thereby indicating the effects of intense photochemistry in summer. Such seasonal pattern is common for most carbonyl species, particularly for n-valeraldehyde, whose concentrations and contributions to total C_1–C_8 carbonyls were largely elevated in summer (1.89 ± 1.28 ppbv and 6.6 ± 2.9%) compared to wintertime (0.09 ± 0.06 ppbv and 0.9 ± 1.2%). An exception was crotonaldehyde, which showed relatively higher concentrations (1.78 ± 1.51 ppbv) and larger contributions (16.1 ± 13.9%) in winter (versus 0.84 ± 1.01 ppbv and 2.9 ± 2.9% in summer). The most abundant carbonyl species varied between seasons. Acetone was the most abundant carbonyl species in winter with an average contribution of 30.4 ± 17.0% (versus 25.3 ± 5.0% in summer), while formaldehyde was the most abundant species in summer with an average contribution of 30.2 ± 4.4% (versus 23.4 ± 8.3% in winter). The distinct seasonal variation patterns for individual species should be related to their complex sources. In particular, the importance of photochemical oxidation in the formation of formaldehyde was underlined.

Fig. 2 presents the average diurnal variations of summed C_1–C_8 carbonyls and major species at the rural site (during 8:00–16:00 LT) in summer and winter. The concentrations of total C_1–C_8 carbonyls exhibited a unimodal diurnal pattern during both seasons, but the exact patterns varied between seasons. For example, the concentrations of total C_1–C_8 carbonyls exhibited a narrow peak at 12:00 LT in summer, while exhibited a broader peak during 10:00–13:00 LT in winter. Such seasonal features were also found in the diurnal patterns of formaldehyde and acetaldehyde. The noon-peak diurnal variation pattern was generally consistent to that of O_3, indicating the significant contributions of photochemistry to carbonyls. In comparison, the concentrations of acetone exhibited bimodal diurnal patterns with two small peaks in the early morning and in the afternoon, respectively, suggesting the influence from both direct emission and photochemical formation. The different diurnal variation patterns among carbonyl species indicate their complex sources, and underline the significant impact of photochemical formation on carbonyls in summer.

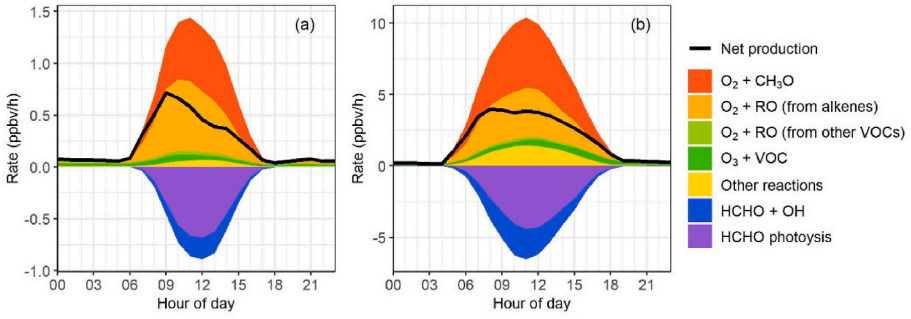

Fig. 3. Breakdown of the chemical production and destruction rates of formaldehyde in (a) winter and (b) summer at the rural site. The results were simulated by the box model. Refer to Section 2.2 for the descriptions of the specific reaction pathways.

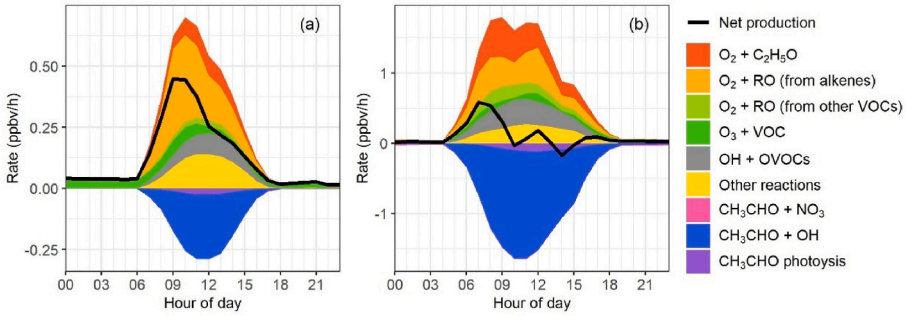

Fig. 4. Breakdown of the chemical production and destruction rates of acetaldehyde in (a) winter and (b) summer at the rural site. The results were simulated by the box model. Refer to Section 2.2 for the descriptions of the specific reaction pathways.

3.2. Formation mechanisms of formaldehyde and acetaldehyde

The aforementioned observation results suggest a significant influence of intense photochemical formation on the carbonyls in the ambient air of YelRD. In this section, we conducted detailed chemical box modeling analyses to quantify the chemical budgets of carbonyl species at the rural site, with formaldehyde and acetaldehyde as examples considering their high abundance and importance to the formation of O_3 and secondary aerosols. A total of eight episodes in winter (i.e., 19, 22, 23, 27, and 28 February and 11, 23, and 29 March 2017) and nine episodes in summer (i.e., 8, 9, 14, 15, 16, 18, 29, and 30 June and 9 July) with available comprehensive measurements were selected to subject to the modeling analyses.

Figs. 3 and 4 present the averaged chemical budget results for formaldehyde and acetaldehyde, respectively, across all selected episodes in summer and winter. At the rural site, the daytime (6:00–18:00 LT) net production rates of formaldehyde were significantly higher in summer (3.00 ± 1.43 ppbv h^{-1}, range: 0.45 ppbv h^{-1} – 9.55 ppbv h^{-1}) than those in winter (0.36 ± 0.39 ppbv h^{-1}, range: -0.07 ppbv h^{-1} – 1.62 ppbv h^{-1}). Comparison with previous studies demonstrated the strong in-situ production of formaldehyde in the rural air of YelRD, which was even larger than that determined in polluted areas such as Beijing and Hong Kong (Yang et al., 2018, 2020). The results indicate the high atmospheric oxidizing capacity in the YelRD region, as the photolysis of formaldehyde was identified as a major primary source of RO_x (OH + HO_2 + RO_2) radicals in our previous paper (Chen et al., 2020). In both summer and winter, the formaldehyde production was governed by the reactions of O_2 + CH_3O (with contributions of

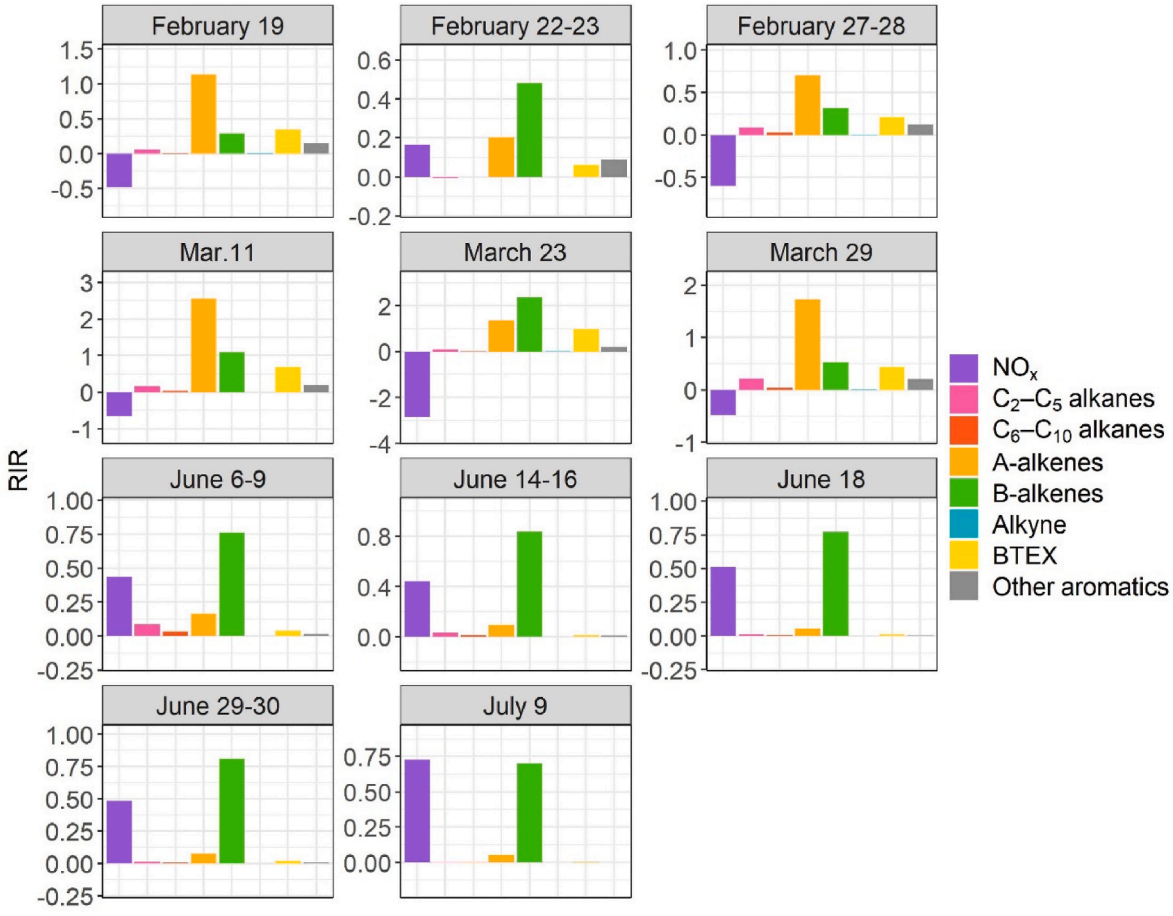

Fig. 5. The model-simulated Relative Incremental Reactivity (RIR) for major formaldehyde precursor groups during selected cases at the rural site.

34.3–48.8%), followed by O_2 + RO (resulting from degradation of alkenes) (26.3–43.7%), while the other three pathways (O_2 + RO (from other VOCs), O_3 + VOCs, and other reactions) made relatively small contributions (totally 18.7–30.1%). The formaldehyde loss was dominated by photolysis (49.8–68.8%) and the reactions with OH (25.4–43.4%). These results illustrate the importance of alkenes (including both anthropogenic and biogenic alkenes) in the secondary formation of formaldehyde, and the relative importance of anthropogenic and biogenic alkenes will be further evaluated by the RIR metrics.

Both the production and destruction rates of acetaldehyde were amplified in summer than in winter (see Fig. 4), leading to comparable daytime (6:00–18:00 LT) net production rates between the two seasons (i.e., 0.17 ± 0.54 ppbv h^{-1}, range: -0.94 ppbv h^{-1} – 3.10 ppbv h^{-1}, in summer versus 0.20 ± 0.23 ppbv h^{-1}, range: 0.00 ppbv h^{-1} – 1.24 ppbv h^{-1}, in winter). Such magnitudes of net rates were higher than those determined in urban Beijing (0.11–0.13 ppbv h^{-1}; Yang et al., 2018), suggesting the active in-situ production of acetaldehyde in the rural air of YelRD. We then explored the detailed chemical budget of acetaldehyde and found some interesting seasonal features. For example, the acetaldehyde production was dominated by the reactions of O_2 + RO (from alkenes) (18.0–48.9%) in winter, but was dominated by the reactions of OH + OVOCs (14.7–32.2%), O_2 + RO (from alkenes) (14.2–25.5%) and $O_2 + C_2H_5O$ (11.2–22.9%) in summer. In both seasons, the acetaldehyde loss was governed by the reactions with OH (84.2–94.5%), while the photolysis and reactions with NO_3 radical made relatively minor contributions (totally 5.5–15.8%). Again, these results underline the relative importance of alkenes (including both anthropogenic and biogenic alkenes) in the secondary formation of acetaldehyde in the YelRD region.

The relationships between major carbonyl species and their precursors were further identified. Considering the relatively low net production rates of acetaldehyde, here we focused on the formaldehyde-precursor relationships. As shown in Fig. 5, RIR was calculated for the major precursors, i.e., NO_x, C_2–C_5 alkanes, C_6–C_{10} alkanes, A-alkenes, B-alkenes, alkyne, BTEX, and other aromatics (see details in Section 2.2). Consistent with the chemical budget analyses, formaldehyde formation was highly sensitive to A-alkenes and B-alkenes. Nonetheless, the exact distributions of RIRs for major precursors varied among different cases and showed some seasonal features. In summer, B-alkenes exhibited the highest positive RIRs (range: 0.70–0.84), followed by NO_x (0.44–0.73) and A-alkenes (0.05–0.17). In comparison, A-alkenes exhibited the highest positive RIRs (0.20–2.57) for most cases in winter. Two exceptions were the episodes on February 22–23 and March 23, when B-alkenes exhibited the highest positive RIRs among major VOC groups. The enhanced importance of B-alkenes in formaldehyde formation should be attributed to the lower concentrations of anthropogenic VOCs than the other winter cases, and attributed to the enhanced isoprene-HCHO yield promoted by high NO_x concentrations (Wolfe et al., 2016). The seasonal variations of RIRs for A-alkenes and B-alkenes are expected as there were strong biogenic emissions at the rural site in summer (e.g., isoprene concentrations: 2.7 ± 1.7 ppbv; Chen et al. (2020)). In addition, the RIRs for NO_x concentrations were generally highly negative (average: -0.82 ± 0.95, range: -2.87 – 0.17) for most winter cases, which should be attributed to the saturated NO_x concentrations in winter.

Both chemical budget analyses and RIR results underline the importance of alkenes (generally anthropogenic alkenes in winter while biogenic alkenes in summer) in the secondary formation of carbonyls in the YelRD region, which is probably also the case for the formation of secondary pollutants such as O_3 and secondary aerosols. However, decreasing the emissions of NO_x by 20% would exert double-edged effects, i.e., promoting the formation of formaldehyde in winter but mitigating the formation of formaldehyde in summer. These findings have useful implications for the formulation of control policy to mitigate regional photochemical air pollution in the YelRD region.

3.3. Comparison of formation mechanisms between rural and oilfield areas

To better understand the formation mechanisms of carbonyls in the oilfield-influenced air of the YelRD region, detailed modeling analyses were conducted for an episode observed on July 9, 2017, when concurrent observations were made both at the rural site and in the oilfield source area. We examined the formation mechanisms of formaldehyde and acetaldehyde from perspectives of in-situ production rates and chemical budgets (Figs. 6 and 7), and relationships with precursors (Fig. 8; for formaldehyde only).

The in-situ production rates of formaldehyde were even larger at the rural site, though its observed concentrations were higher at the oilfield site (Fig. 6). The former should be caused by the stronger biogenic VOC emissions at the rural site (e.g., isoprene concentrations of 2.7 ± 1.7 ppbv vs. 0.9 ± 0.7 ppbv at the oilfield site), and the latter might be related to the stronger direct emissions of formaldehyde from pumpjacks at the oilfield site (Barickman and Lyman, 2015). The chemical budgets of formaldehyde were similar between two sites, and were generally the same to the summer-averaged results at the rural site. Quantitatively, the production was dominated by the reactions of O_2 + CH_3O (rural: 41.5%; oilfield: 47.2%) and O_2 + RO (from alkenes) (rural: 31.1%; oilfield: 37.2%), and the loss was dominated by photolysis (rural: 67.6%; oilfield: 53.4%) and the reactions with OH (rural: 32.3%; oilfield: 46.4%). Nevertheless, the key precursors of formaldehyde differed somewhat between the two sites (Fig. 8). At the rural site, formaldehyde formation was most sensitive to NO_x (RIR: 0.73), followed by B-alkenes (RIR: 0.70). The other hydrocarbon groups showed relatively smaller RIR values (<0.05). In comparison, formaldehyde formation was most sensitive to B-alkenes (RIR: 0.58) and NO_x (RIR: 0.29) at the oilfield site. In addition, the sensitivity of formaldehyde formation to anthropogenic hydrocarbons increased (e.g., the RIRs for A-alkenes was 0.21) due to strong VOCs emissions in the oilfield area.

For acetaldehyde, both the in-situ production rates and observed concentrations were larger at the oilfield site than at the rural site (Fig. 7). The results suggest the significant impact of anthropogenic

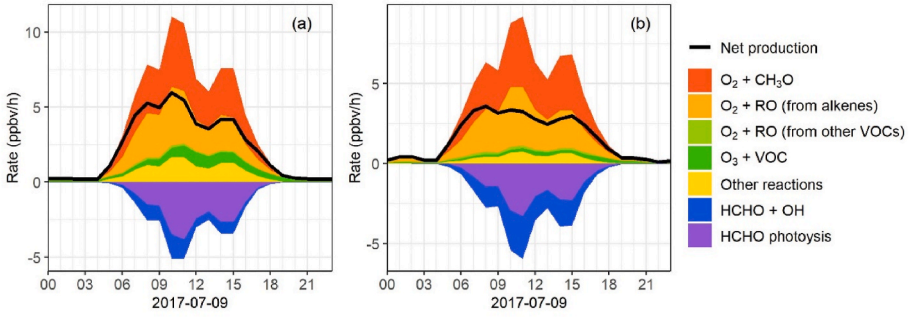

Fig. 6. Breakdown of the chemical production and destruction rates of formaldehyde on July 9, 2017 (a) at the rural site and (b) at the oilfield source site. The results were simulated by the box model. Refer to Section 2.2 for the descriptions of the specific reaction pathways.

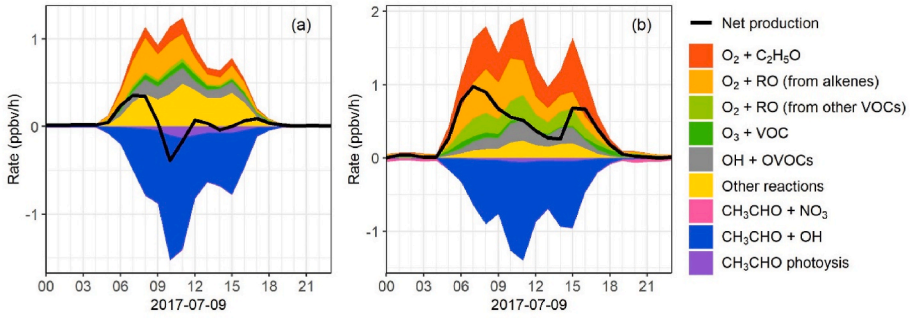

Fig. 7. Breakdown of the chemical production and destruction rates of acetaldehyde on July 9, 2017 (a) at the rural site and (b) at the oilfield source site. The results were simulated by the box model. Refer to Section 2.2 for the descriptions of the specific reaction pathways.

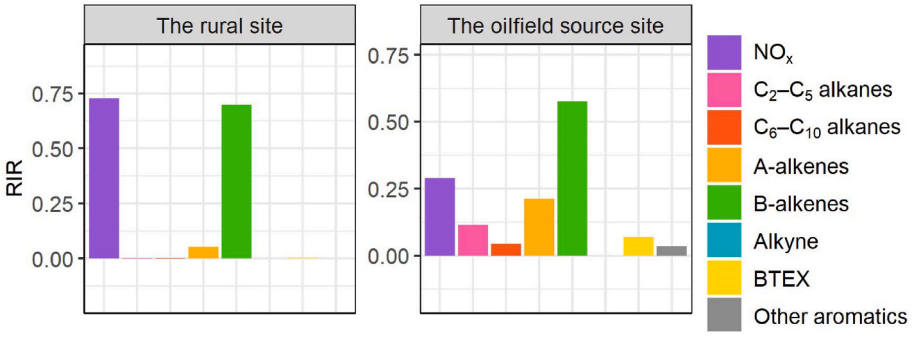

Fig. 8. The model-simulated RIRs for major formaldehyde precursor groups on July 9, 2017 (a) at the rural site and (b) at the oilfield source site.

(oilfield) emissions on acetaldehyde formation. The chemical budgets of acetaldehyde were partly different between the two sites. At the rural site, the cross-radical reactions (28.8%) and O_2 + RO (from alkenes) (22.7%) made the largest contributions to the acetaldehyde production on 9 July, which is different from the summer-averaged results that OH + VOCs (25.7 ± 5.1%) and O_2 + RO (from alkenes) (20.2 ± 3.8%) made the largest contributions. The enhancement of cross-radical reactions indicated a more aged air mass at the rural site on July 9. In comparison, the acetaldehyde production at the oilfield source site was dominated by the reactions of O_2 + C_2H_5O (34.4%) and O_2 + RO (from alkenes) (23.3%). At both sites, the acetaldehyde loss was dominated by the reactions with OH (rural: 92.7%; oilfield: 95.8%).

Overall, the above results illustrated the effects of oilfield emissions on the formation mechanisms of formaldehyde and acetaldehyde. The strong oilfield emissions on one hand led to higher sensitivities of formaldehyde to anthropogenic hydrocarbons, and on the other hand prompted the secondary formation of acetaldehyde with abundant precursors.

4. Conclusions

In this work, we analyzed the characteristics and formation mechanisms of C_1–C_8 carbonyls at two sites (rural and oilfield) in the Yellow River Delta region, northern China, in winter and summer 2017. The observed concentrations of C_1–C_8 carbonyls in the oilfield were higher than those in the rural area, demonstrating the effects of oilfield emissions. Both seasonal and diurnal variations of C_1–C_8 carbonyls indicated a significant influence of secondary formation, as which showed higher concentration levels in summer than in winter and showed well-defined patterns with a concentration peak in the afternoon. The MCM chemical box model was used to quantify the in-situ production rates, chemical budgets, and relationships with precursors for major carbonyl compounds. The strong in-situ production of formaldehyde and acetaldehyde in the YelRD region was demonstrated, and alkenes were found to make important contributions through the pathway of O_2 + RO reactions. The strong oilfield emissions do affect the formation mechanisms of carbonyls. A larger in-situ production rate of acetaldehyde and higher sensitivity of formaldehyde formation to anthropogenic hydrocarbons were determined at the oilfield source site compared to that at the rural site. Overall, this study highlights the impact of oilfield emissions on the ambient carbonyls and atmospheric photochemistry in the oilfield areas.

CRediT authorship contribution statement

Tianshu Chen: organized the experiments, conducted the field measurements, concentrations in the samples, analyzed the data, wrote and revised the paper. **Penggang Zheng:** conducted the field measurements. **Yingnan Zhang:** wrote and revised the paper. **Can Dong:** wrote and revised the paper. **Guangxuan Han:** provided resources for field measurement and sample analysis, reviewed the paper and provided helpful comments. **Hong Li:** provided resources for field measurement and sample analysis, reviewed the paper and provided helpful comments. **Xue Yang:** analyzed the data. **Yuhong Liu:** conducted the field measurements. **Jingjing Sun:** conducted the field measurements. **Hongyong Li:** conducted the field measurements. **Xin Zhang:** measured the carbonyls concentrations in the samples. **Yunfeng Li:** measured . **Wenxing Wang:** reviewed the paper and provided helpful comments. **Likun Xue:** designed and supervised the experiments, provided resources for field measurement and sample analysis, reviewed the paper and provided helpful comments.

Declaration of competing interest

The authors declare that they have no known competing financial interests or personal relationships that could have appeared to influence the work reported in this paper.

Acknowledgments

The authors thank Mr. Changli Yang and Dr. Rui Li for their help in the field studies. We thank the University of Leeds for providing the Master

Chemical Mechanism (version 3.3.1) and Glenn M. Wolfe for providing the Framework for 0-D Atmospheric Modeling (F0AM). This work was funded by the Shandong Provincial Science Foundation for Distinguished Young Scholars (ZR2019JQ09), the National Natural Science Foundation of China (41675118, 41922051 and 41905113), National research program for key issues in air pollution control (DQGG202121) and the Jiangsu Collaborative Innovation Center for Climate Change.

Appendix A. Supplementary data

Supplementary data to this article can be found online at https://doi.org/10.1016/j.atmosenv.2022.118958.

References

Adgate, J.L., Goldstein, B.D., McKenzie, L.M., 2014. Potential public health hazards, exposures and health effects from unconventional natural gas development. Environ. Sci. Technol. 48, 8307–8320. https://doi.org/10.1021/es404621d.

Ahmadov, R., McKeen, S., Trainer, M., Banta, R., Brewer, A., Brown, S., Edwards, P.M., Gouw, J.A. de, Frost, G.J., Gilman, J., Helmig, D., Johnson, B., Karion, A., Koss, A., Langford, A., Lerner, B., Olson, J., Oltmans, S., Peischl, J., Pétron, G., Pichugina, Y., Roberts, J.M., Ryerson, T., Schnell, R., Senff, C., Sweeney, C., Thompson, C., Veres, P.R., Warneke, C., Wild, R., Williams, E.J., Yuan, B., Zamora, R., 2015. Understanding high wintertime ozone pollution events in an oil- and natural gas-producing region of the western US. Atmos. Chem. Phys. 15, 411–429. https://doi.org/10.5194/acp-15-411-2015.

Bao, J., Li, H., Wu, Z., Zhang, X., Zhang, H., Li, Y., Qian, J., Chen, J., Deng, L., 2022. Atmospheric carbonyls in a heavy ozone pollution episode at a metropolis in Southwest China: characteristics, health risk assessment, sources analysis. J Environ Sci 113, 40–54. https://doi.org/10.1016/j.jes.2021.05.029.

Barickman, P., Lyman, S., 2015. Measurement of carbonyl emissions from oil and gas sources in the Uintah Basin. URL. https://www.usu.edu/binghamresearch/files/CarbonylEmiss-FnlRprt-31jul2015.pdf. (Accessed 7 May 2021).

British Petroleum Company plc, 2020. BP Statistical Review of World Energy 2020. URL. https://www.bp.com/en/global/corporate/energy-economics/statistical-review-of-world-energy.html. (Accessed 7 May 2021).

Chen, T., Xue, L., Zheng, P., Zhang, Y., Liu, Y., Sun, J., Han, G., Li, H., Zhang, X., Li, Y., Li, Hong, Dong, C., Xu, F., Zhang, Q., Wang, W., 2020. Volatile organic compounds and ozone air pollution in an oil production region in northern China. Atmos. Chem. Phys. 20, 7069–7086. https://doi.org/10.5194/acp-20-7069-2020.

Cheng, Y., Lee, S., Huang, Y., Ho, K.F., Ho, S.S.H., Yau, P.S., Louie, P.K.K., Zhang, R., 2014. Diurnal and seasonal trends of carbonyl compounds in roadside, urban, and suburban environment of Hong Kong. Atmos. Environ. 89, 43–51. https://doi.org/10.1016/j.atmosenv.2014.02.014.

Colborn, T., Schultz, K., Herrick, L., Kwiatkowski, C., 2013. An exploratory study of air quality near natural gas operations. Hum. Ecol. Risk Assess. 20, 86–105. https://doi.org/10.1080/10807039.2012.749447.

Edwards, P.M., Brown, S.S., Roberts, J.M., Ahmadov, R., Banta, R.M., deGouw, J.A., Dubé, W.P., Field, R.A., Flynn, J.H., Gilman, J.B., Graus, M., Helmig, D., Koss, A., Langford, A.O., Lefer, B.L., Lerner, B.M., Li, R., Li, S.-M., McKeen, S.A., Murphy, S. M., Parrish, D.D., Senff, C.J., Soltis, J., Stutz, J., Sweeney, C., Thompson, C.R., Trainer, M.K., Tsai, C., Veres, P.R., Washenfelder, R.A., Warneke, C., Wild, R.J., Young, C.J., Yuan, B., Zamora, R., 2014. High winter ozone pollution from carbonyl photolysis in an oil and gas basin. Nature 514, 351. https://doi.org/10.1038/nature13767.

EIA (Energy Information Administration), 2021a. Total Energy Production from Natural Gas 2018. URL. https://www.eia.gov/international/rankings/world?pa=287&u=0&f=A&v=none&y=01%2F01%2F2018. (Accessed 7 May 2021).

EIA (Energy Information Administration), 2021b. Total Energy Production from Petroleum and Other Liquids 2018. URL. https://www.eia.gov/international/rankings/world?pa=288&u=0&f=A&v=none&y=01%2F01%2F2018. (Accessed 7 May 2021).

Field, R.A., Soltis, J., McCarthy, M.C., Murphy, S., Montague, D.C., 2015. Influence of oil and gas field operations on spatial and temporal distributions of atmospheric non-methane hydrocarbons and their effect on ozone formation in winter. Atmos. Chem. Phys. 15, 3527–3542. https://doi.org/10.5194/acp-15-3527-2015.

He, Z., Zhang, X., Li, Y., Zhong, X., Li, H., Gao, R., Li, J., 2020. Characterizing carbonyl compounds and their sources in Fuzhou ambient air, southeast of China. PeerJ 8, e10227. https://doi.org/10.7717/peerj.10227.

Huang, X., Zhang, B., Xia, S., Han, Y., Wang, C., Yu, G., Feng, N., 2020. Sources of oxygenated volatile organic compounds (OVOCs) in urban atmospheres in North and South China. Environ. Pollut. 114152 https://doi.org/10.1016/j.envpol.2020.114152.

Jiang, Z., Grosselin, B., Daële, V., Mellouki, A., Mu, Y., 2016. Seasonal, diurnal and nocturnal variations of carbonyl compounds in the semi-urban environment of Orléans, France. J Environ Sci 40, 84–91. https://doi.org/10.1016/j.jes.2015.11.016.

Liu, Y., Wang, H., Jing, S., Gao, Y., Peng, Y., Lou, S., Cheng, T., Tao, S., Li, L., Li, Y., Huang, D., Wang, Q., An, J., 2019. Characteristics and sources of volatile organic compounds (VOCs) in Shanghai during summer: implications of regional transport. Atmos. Environ. 215, 116902 https://doi.org/10.1016/j.atmosenv.2019.116902.

Liu, Z., Cui, Y., He, Q., Guo, L., Gao, X., Feng, Y., Wang, Y., Wang, X., 2021. Seasonal variations of carbonyls and their contributions to the ozone formation in urban atmosphere of taiyuan, China. Atmosphere 12, 510. https://doi.org/10.3390/atmos12040510.

McDonald, B.C., Gouw, J.A. de, Gilman, J.B., Jathar, S.H., Akherati, A., Cappa, C.D., Jimenez, J.L., Lee-Taylor, J., Hayes, P.L., McKeen, S.A., Cui, Y.Y., Kim, S.-W., Gentner, D.R., Isaacman-VanWertz, G., Goldstein, A.H., Harley, R.A., Frost, G.J., Roberts, J.M., Ryerson, T.B., Trainer, M., 2018. Volatile chemical products emerging as largest petrochemical source of urban organic emissions. Science 359, 760–764. https://doi.org/10.1126/science.aaq0524.

McDuffie, E.E., Edwards, P.M., Gilman, J.B., Lerner, B.M., Dubé, W.P., Trainer, M., Wolfe, D.E., Angevine, W.M., deGouw, J., Williams, E.J., Tevlin, A.G., Murphy, J.G., Fischer, E.V., McKeen, S., Ryerson, T.B., Peischl, J., Holloway, J.S., Aikin, K., Langford, A.O., Senff, C.J., Alvarez, R.J., Hall, S.R., Ullmann, K., Lantz, K.O., Brown, S.S., 2016. Influence of oil and gas emissions on summertime ozone in the Colorado Northern Front Range. J. Geophys. Res. Atmos. 121, 8712–8729. https://doi.org/10.1002/2016jd025265.

Mellouki, A., Wallington, T.J., Chen, J., 2015. Atmospheric chemistry of oxygenated volatile organic compounds: impacts on air quality and climate. Chem. Rev. 115, 3984–4014. https://doi.org/10.1021/cr500549n.

Michoud, V., Sciare, J., Sauvage, S., Dusanter, S., Léonardis, T., Gros, V., Kalogridis, C., Zannoni, N., Féron, A., Petit, J.-E., Crenn, V., Baisnée, D., Sarda-Estève, R., Bonnaire, N., Marchand, N., DeWitt, H.L., Pey, J., Colomb, A., Gheusi, F., Szidat, S., Stavroulas, I., Borbon, A., Locoge, N., 2017. Organic carbon at a remote site of the western Mediterranean Basin: sources and chemistry during the ChArMEx SOP2 field experiment. Atmos. Chem. Phys. 17, 8837–8865. https://doi.org/10.5194/acp-17-8837-2017.

Mu, Y., Pang, X., Quan, J., Zhang, X., 2007. Atmospheric carbonyl compounds in Chinese background area: a remote mountain of the Qinghai-Tibetan Plateau. J. Geophys. Res. Atmos. 112 https://doi.org/10.1029/2006jd008211, 1984 2012.

Nogueira, T., Dominutti, P.A., Fornaro, A., Andrade, M., de, F., 2017. Seasonal trends of formaldehyde and acetaldehyde in the megacity of São Paulo. Atmos.-basel 8, 144. https://doi.org/10.3390/atmos8080144.

Qian, X., Shen, H., Chen, Z., 2019. Characterizing summer and winter carbonyl compounds in Beijing atmosphere. Atmos. Environ. 214, 116845 https://doi.org/10.1016/j.atmosenv.2019.116845.

Saunders, S.M., Jenkin, M.E., Derwent, R.G., Pilling, M.J., 2003. Protocol for the development of the Master Chemical Mechanism, MCM v3 (Part A): tropospheric degradation of non-aromatic volatile organic compounds. Atmos. Chem. Phys. 3, 161–180. https://doi.org/10.5194/acp-3-161-2003.

Villanueva, F., Lara, S., Amo-Salas, M., Cabañas, B., Martín, P., Salgado, S., 2021. Investigation of formaldehyde and other carbonyls in a small urban atmosphere using passive samplers. A comprehensive data analysis. Microchem. J. 167, 106270 https://doi.org/10.1016/j.microc.2021.106270.

Wang, J., Sun, S., Zhang, C., Xue, C., Liu, P., Zhang, C., Mu, Y., Wu, H., Wang, D., Chen, H., Chen, J., 2020. The pollution levels, variation characteristics, sources and implications of atmospheric carbonyls in a typical rural area of North China Plain during winter. J Environ Sci. https://doi.org/10.1016/j.jes.2020.05.003.

Wolfe, G.M., Marvin, M.R., Roberts, S.J., Travis, K.R., Liao, J., 2016. The Framework for 0-D atmospheric modeling (F0AM) v3.1. Geosci. Model Dev. (GMD) 9, 3309–3319. https://doi.org/10.5194/gmd-9-3309-2016.

Wu, C., Wang, C., Wang, S., Wang, W., Yuan, B., Qi, J., Wang, B., Wang, H., Wang, C., Song, W., Wang, X., Hu, W., Lou, S., Ye, C., Peng, Y., Wang, Z., Huangfu, Y., Xie, Y., Zhu, M., Zheng, J., Wang, X., Jiang, B., Zhang, Z., Shao, M., 2020. Measurement report: important contributions of oxygenated compounds to emissions and chemistry of volatile organic compounds in urban air. Atmos. Chem. Phys. 20, 14769–14785. https://doi.org/10.5194/acp-20-14769-2020.

Xue, L., Gu, R., Wang, T., Wang, X., Saunders, S., Blake, D., Louie, P.K.K., Luk, C.W.Y., Simpson, I., Xu, Z., Wang, Z., Gao, Y., Lee, S., Mellouki, A., Wang, W., 2016. Oxidative capacity and radical chemistry in the polluted atmosphere of Hong Kong and Pearl River Delta region: analysis of a severe photochemical smog episode. Atmos. Chem. Phys. 16, 9891–9903. https://doi.org/10.5194/acp-16-9891-2016.

Xue, L., Saunders, S.M., Wang, T., Gao, R., Wang, X., Zhang, Q., Wang, W., 2015. Development of a chlorine chemistry module for the master chemical mechanism. Geosci. Model Dev. (GMD) 8, 3151–3162. https://doi.org/10.5194/gmd-8-3151-2015.

Yang, X., Xue, L., Wang, T., Wang, X., Gao, J., Lee, S., Blake, D.R., Chai, F., Wang, W., 2018. Observations and explicit modeling of summertime carbonyl formation in Beijing: identification of key precursor species and their impact on atmospheric oxidation chemistry. J. Geophys. Res. Atmos. 123, 1426–1440. https://doi.org/10.1002/2017jd027403.

Yang, X., Zhang, G., Sun, Y., Zhu, L., Wei, X., Li, Z., Zhong, X., 2020. Explicit modeling of background HCHO formation in southern China. Atmos. Res., 104941 https://doi.org/10.1016/j.atmosres.2020.104941.

Ye, C., Yuan, B., Lin, Y., Wang, Z., Hu, W., Li, T., Chen, W., Wu, C., Wang, C., Huang, S., Qi, J., Wang, B., Wang, C., Song, W., Wang, X., Zheng, E., Krechmer, J.E., Ye, P., Zhang, Z., Wang, X., Worsnop, D.R., Shao, M., 2021. Chemical characterization of oxygenated organic compounds in the gas phase and particle phase using iodide CIMS with FIGAERO in urban air. Atmos. Chem. Phys. 21, 8455–8478. https://doi.org/10.5194/acp-21-8455-2021.

Zhang, Y., Xue, L., Dong, C., Wang, T., Mellouki, A., Zhang, Q., Wang, W., 2019. Gaseous carbonyls in China's atmosphere: tempo-spatial distributions, sources, photochemical formation, and impact on air quality. Atmos. Environ. 214, 116863 https://doi.org/10.1016/j.atmosenv.2019.116863.